

Boundary Conditions for the Finite Difference Beam Propagation Method based on Plane Wave Solutions of the Fresnel Equation

M. Lohmeyer, M. Shamonin and P. Hertel

Abstract— Each particular implementation of the beam propagation method (BPM) requires a special procedure allowing for radiation to leave the computational window. We propose a new approach to constructing the finite difference schemes of the BPM at the boundary of the computational window. These schemes are independent of the computed fields and allow for a similar treatment of both interior and boundary points. The new approach can be further improved by correcting the field values at the boundary points according to Hadley's method. The algorithm is easy to implement for both two- and three-dimensional structures. The new method considerably reduces computation times because the propagation matrices remain constant in longitudinally invariant sections, thus avoiding repeated LU-decompositions. The basic idea – establishing the finite difference scheme such that locally exact, approximate or plausible solutions are recovered – may be of interest for other efforts to solve partial differential equations by the finite difference method.

Keywords— integrated optics, beam propagation method, transparent boundary conditions, finite differences

I. INTRODUCTION

WITHIN the framework of the beam propagation method (BPM) [1] standard boundary conditions do not provide satisfactory results. The power on the transverse computational window is conserved if the field or the derivative in the normal direction on the boundary are prescribed. A method is required which models an unbounded computational domain. Several possibilities have been proposed:

- Absorbing boundary conditions [2], [3]: A refractive index with an imaginary part is used close to the boundary. One has to choose the shape of these absorbing zones carefully. A considerable part of the discretization points is wasted for the boundary, especially in 3-D simulations.
- Integration methods [4], [5], [6]: They are based on the description of the boundary fields in terms of Green's functions. For each propagation step integrations over the computed fields at the boundary are necessary. Formulas are available only for 2-D simulations.
- Transparent Boundary Conditions TBC [7], [8]: The field next to the boundary is assumed to depend exponentially on the transverse coordinate. After each propagation step the outermost field values and some entries in the propagation matrices are corrected according to this assumption. The method is easily implemented and works well (however, see Ref. [6] for

precautions).

- A hybrid method [9]: The absorber technique and the TBC are implemented simultaneously, with a field dependent shape of the absorber profile.

FD-BPM indicates beam propagation calculations based on the approximation of derivatives by finite differences. In most cases the propagation equation is developed from Maxwell's equations in paraxial approximation. For each propagation step, a system of linear equations has to be solved. The corresponding large matrices are sparse, but not necessarily tridiagonal [10], [11], [12].

The paraxial approximation is valid only for structures which are varying but slowly in the direction of propagation. They can be divided into longitudinally invariant sections. Usually, for each section, several or many steps are required. For calculations reported in this paper the routines of the SPARSE package [13] were employed to solve the linear system of equations. First the propagation matrix is decomposed into two triangular matrices, then the new field values are evaluated by backsubstitution. For a 3-D vectorial simulation, decomposition is typically 100 times as expensive (in time) than backsubstitution. It is therefore highly desirable to work with constant propagation matrices whenever possible. Recall that the method of transparent boundary conditions (TBC) modifies the propagation matrix after each step, even if the structure is homogeneous.

II. WAVE EQUATION AND FINITE DIFFERENCES

We choose a Cartesian coordinate system x, y, z where x, y denote the transverse and z the longitudinal (propagation) coordinates. All field components are of the form

$$\Psi(t, x, y, z) = \psi(x, y, z) \exp i(\omega t - kn_r z), \quad (1)$$

where ω is the angular frequency of light, $k = 2\pi/\lambda$ the vacuum wavenumber and n_r a reference refractive index.

On the boundary of the transverse computational window a piecewise constant and diagonal permittivity with local refractive index n is assumed. Then, in the paraxial approximation, the slowly varying amplitudes ψ obey the Fresnel equation

$$\frac{\partial \psi}{\partial z} = \frac{ik}{2n_r} (n_r^2 - n^2) \psi - \frac{i}{2kn_r} \left(\frac{\partial^2}{\partial x^2} + \frac{\partial^2}{\partial y^2} \right) \psi. \quad (2)$$

Many BPM algorithms rely on the finite-difference approximation of this equation. Discretization of Eq. (2) with respect to the transverse coordinates in a conventional way leads to the following finite difference scheme:

The authors are with the Department of Physics, University of Osnabrück, Barbarastrasse 7, D-49069 Osnabrück, Germany

$$\begin{aligned} \left(\frac{\partial\psi}{\partial z}\right)_{a,b} &= \frac{ik}{2n_r}(n_r^2 - n^2)\psi_{a,b} \\ &- \frac{i}{2kn_r}\left(\frac{1}{\Delta x^2}(\psi_{a+1,b} - 2\psi_{a,b} + \psi_{a-1,b})\right. \\ &\quad \left. + \frac{1}{\Delta y^2}(\psi_{a,b+1} - 2\psi_{a,b} + \psi_{a,b-1})\right) \end{aligned} \quad (3)$$

A subscript (a, b) denotes values at the point $(x, y) = (a\Delta x, b\Delta y)$, $a = 1, \dots, N_x$, $b = 1, \dots, N_y$ of a rectangular computational window. Obviously, the scheme (3) can be used only at interior points $1 < a < N_x$, $1 < b < N_y$. At a boundary point Eq. (3) has to be supplemented by an expression for the longitudinal derivative in terms of field values in its neighbourhood. In Section IV this problem is tackled by a procedure based on paraxial plane wave solutions of the Fresnel equation (2). The idea behind this approach can be explained best by a simple example presented in the following Section.

Equation (3) may be written in matrix form

$$\mathbf{A}\frac{\partial\psi}{\partial z} = \mathbf{B}\psi, \quad (4)$$

where the vector ψ is built from the $N_x \times N_y$ functions $\psi_{a,b}(z)$. Further discretization in the longitudinal direction results in a system of linear equations connecting the discretized fields at planes $z = s\Delta z$ and $z = (s+1)\Delta z$:

$$\left(\frac{1}{\Delta z}\mathbf{A} - \alpha\mathbf{B}\right)\psi^{s+1} = \left(\frac{1}{\Delta z}\mathbf{A} + (1-\alpha)\mathbf{B}\right)\psi^s. \quad (5)$$

The scheme is stable only for $1/2 \leq \alpha \leq 1$ [10]. For $\alpha = 1/2$ (5) is the Crank Nicolson scheme.

Note that we allow for matrix \mathbf{A} to differ from the unity matrix. This situation occurs for certain fully vectorial calculations, in anisotropic media [12], or if alternative formulations are employed [14], [15].

In a longitudinally homogeneous structure the permittivities incorporated in (3) remain constant, a longitudinally varying structure will be approximated by z -invariant sections. Therefore the matrices \mathbf{A} and \mathbf{B} do not depend on the z discretization index.

III. DIFFERENCE SCHEMES FROM SOLUTIONS: AN EXAMPLE

We look for the discrete values $u_k = u(k\Delta t)$ of the solution u of the harmonic equation

$$\frac{\partial^2 u}{\partial t^2} + \omega^2 u = 0 \quad (6)$$

with given consecutive values u_0, u_1 . Conventional discretization (i.e. replacing u_k'' by $(u_{k+1} - 2u_k + u_{k-1})/\Delta t^2$) leads to an approximate formula which expresses u_{k+1} as a linear combination of u_k and u_{k-1} : $u_{k+1} = (2 - \omega^2\Delta t^2)u_k - u_{k-1}$. The differential equation has become a recursion relation.

Motivated by this result, we assume a recursion relation of second order:

$$u_{k+1} = c_1 u_k + c_2 u_{k-1}.$$

The coefficients c_1, c_2 are to be determined. We demand that the known solutions of our differential equation, namely $v(t) = \exp(-i\omega t)$ and $w(t) = \exp(i\omega t)$, must be reproduced by the difference scheme. v and w are called generating functions because they will be used to generate optimal coefficients c_1 and c_2 . We introduce a function D to measure the deviation between the exact values of the generating functions from values calculated with the guessed scheme:

$$\begin{aligned} D(c_1, c_2) &= |v_{k+1} - (c_1 v_k + c_2 v_{k-1})|^2 \\ &\quad + |w_{k+1} - (c_1 w_k + c_2 w_{k-1})|^2 \\ &= |c_1 + c_2 \exp(i\omega\Delta t) - \exp(-i\omega\Delta t)|^2 \\ &\quad + |c_1 + c_2 \exp(-i\omega\Delta t) - \exp(i\omega\Delta t)|^2. \end{aligned}$$

The minimum of D provides optimal coefficients $c_1 = 2 \cos \omega\Delta t$ and $c_2 = -1$. This finite difference scheme,

$$u_{k+1} = (2 \cos \omega\Delta t)u_k - u_{k-1},$$

results in exact solutions of equation (6).

Note that for $\Delta t \rightarrow 0$ we obtain the conventional finite difference scheme which gives only an approximation to the exact solution. To summarize: exact, approximate or plausible solutions of a particular differential equation may serve to obtain the finite difference scheme for solving it.

IV. DIFFERENCE SCHEMES AT THE BOUNDARY

The least-squares procedure sketched in the preceding Section can be used to generate the difference schemes for the boundary of the computational window. As in Eq. (3) the longitudinal derivative shall depend linearly on the field values at neighbouring points:

$$\left(\frac{\partial\psi}{\partial z}\right)_{a,b} = \sum_{j=1}^J c_j \psi_{a+a_j, b+b_j} \quad (7)$$

The form of the mesh stencils is determined by the index differences a_j, b_j , $j = 1, \dots, J$. Fig. 1 shows plausible stencils while Tab. I gives the corresponding index differences. It is seen that the usual five-, four- and three-point stencils have been used at interior, boundary, and corner points, respectively.

Eq. (7) must be able to model paraxial solutions of Maxwell's equations in an isotropic, homogeneous and linear medium. Furthermore, the generating functions should represent outgoing radiation. Therefore a set of properly selected plane waves is the natural choice:

$$\begin{aligned} F^{lm}(x, y, z) &= \exp\left(ik\left(\left(\frac{n_r}{2} - \frac{n^2}{2n_r} \cos \theta_l\right)z\right.\right. \\ &\quad \left.\left. - \left(\frac{n}{\sqrt{2}} \sin \theta_l \cos \varphi_m\right)x - \left(\frac{n}{\sqrt{2}} \sin \theta_l \sin \varphi_m\right)y\right)\right), \end{aligned} \quad (8)$$

where the two superscripts l, m correspond to the polar angle θ_l and the azimuthal angle φ_m with respect to the z -coordinate. The functions F^{lm} satisfy Eq. (2) for small θ_l up to the third order in θ_l . Moreover, it turns out that

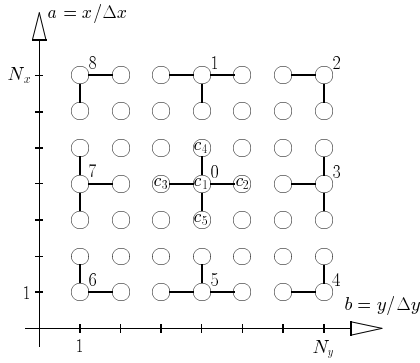


Fig. 1. Possible stencils for the 3-D case. Joined points belong to the same scheme. The numbers indicate the type of boundary point, 0 denotes an interior point.

TABLE I
INDEX DIFFERENCES FOR THE STENCILS OF FIG. 1.

Typ	J	a_1, b_1	a_2, b_2	a_3, b_3	a_4, b_4	a_5, b_5
0	5	0,0	0,1	0,-1	1,0	-1,0
1	4	0,0	0,1	0,-1	-1,0	
2	3	0,0	0,-1	-1,0		
3	4	0,0	1,0	-1,0	0,-1	
4	3	0,0	0,-1	1,0		
5	4	0,0	0,1	0,-1	1,0	
6	3	0,0	1,0	0,-1		
7	4	0,0	1,0	-1,0	0,1	
8	3	0,0	-1,0	0,1		

with such a choice the deviation function D defined below is independent of the coordinates. A finite set of $N_\theta \times N_\varphi$ generating functions is given by

$$\theta_l = l\theta_{max}/N_\theta, \quad l = 0, \dots, N_\theta, \quad (9)$$

$$\varphi_m = \varphi_{min} + m(\varphi_{max} - \varphi_{min})/N_\varphi, \quad m = 0, \dots, N_\varphi.$$

We define the deviation function as

$$D(c_1, \dots, c_J) = \sum_{l,m} g_{lm}^2 \left| \left(\frac{\partial F^{lm}}{\partial z} \right)_{a,b} - \sum_{j=1}^J c_j F_{a+a_j, b+b_j}^{lm} \right|^2, \quad (10)$$

where the weights g_{lm} are given by

$$g_{lm} = \exp(-(\theta_l - \theta_{opt})^2 / \theta_w^2). \quad (11)$$

θ_{opt} and θ_w are additional parameters to be adjusted. Generating functions with a polar angle close to θ_{opt} contribute strongly to D . Guidelines how to select these parameters are discussed in Section V.

The coefficients c_j have to minimize D :

$$\frac{\partial D}{\partial \text{Rec}_j} = 0, \quad \frac{\partial D}{\partial \text{Imc}_j} = 0, \quad (12)$$

or

$$\sum_{k=1}^J L_{jk} c_k = R_j, \quad j = 1, \dots, J$$

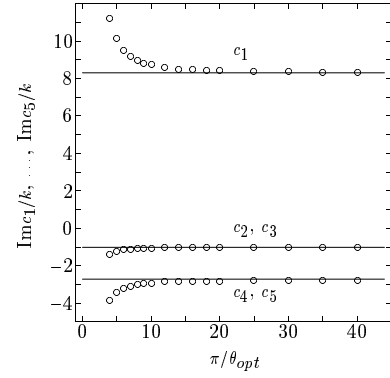


Fig. 2. Imaginary parts of the coefficients $c_1/k, \dots, c_5/k$ versus the reciprocal polar angle π/θ_{opt} as calculated from Eq. (12). The real parts of all coefficients were smaller than 10^{-14} . Lines show the values of Eq. (3). Parameters: $n = 1$, $n_r = 2$, $\Delta x = 0.3/k$, $\Delta y = 0.5/k$, $\theta_{max} = \pi/4$, $\theta_w = \pi/60$, $N_\theta = 100$, $\varphi_{min} = 0$, $\varphi_{max} = 2\pi$, $N_\varphi = 80$.

TABLE II
SECTIONS OF THE AZIMUTHAL ANGLE φ FOR THE GENERATING FUNCTIONS.

Typ	0	1	2	3	4	5	6	7	8
φ_{min}	0	$-\pi/2$	0	0	$\pi/2$	$\pi/2$	π	π	$3\pi/2$
φ_{max}	2π	$\pi/2$	$\pi/2$	π	π	$3\pi/2$	$3\pi/2$	2π	2π

where

$$L_{jk} = \sum_{l,m} g_{lm}^2 (F_{a+a_j, b+b_j}^{lm})^* (F_{a+a_k, b+b_k}^{lm}),$$

$$R_j = \sum_{l,m} g_{lm}^2 (F_{a+a_j, b+b_j}^{lm})^* \left(\frac{\partial F^{lm}}{\partial z} \right)_{a,b}.$$

Let us first consider an interior point (type 0 in Tab. I). In the limit $\theta_{opt} \rightarrow 0$ Eq. (12) leads to the usual finite difference scheme Eq. (3) as can easily be seen from Fig. 2. Our method of minimizing the error (10) is capable of reproducing the conventional finite difference scheme for the Fresnel equation in a homogeneous medium.

The coefficients c_j for the boundary points can be calculated similarly. To forbid reflection at the boundary one has to consider only such waves that do not propagate towards the interior of the computational window [8]. In the framework of our method this can be achieved easily by setting parameters φ_{min} , φ_{max} as shown in Tab. II. For boundary points, the missing equations of the form (3) are obtained as solutions of Eq. (12), separately for each boundary point type and for each refractive index.

It is usually sufficient to work with scalar difference schemes even if there are refractive index discontinuities along the boundary. For fully vectorial computations, the field components are usually uncoupled in the boundary region. All components satisfy the same wave equation. Therefore, one scalar difference scheme is built into the

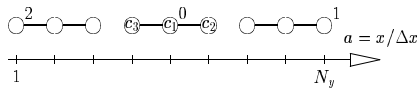


Fig. 3. Stencils in the 2-D case.

 TABLE III
 INDEX DIFFERENCES FOR THE STENCILS OF FIG. 3.

Typ	J	a_1	a_2	a_3
0	3	0	1	-1
1	3	0	-1	-2
2	3	0	1	2

propagation matrices for each field component at each boundary point.

With a properly modified set of generating functions (8) our approach can easily be applied to the two-dimensional case (i.e. one transversal coordinate). The second superscript is to be dropped, φ is set to zero and θ_{max} and θ_{opt} get a sign depending on the boundary point. It turns out that the stencils connecting the boundary points with the two neighbouring grid points (see Fig. 3) provide better boundary transparency.

We have found out that the reflectivity of the new boundary conditions is further reduced if fields are corrected according to steps 1) and 2) of Hadleys TBC-algorithm, see Section II.C in Ref. [8]. This correction takes place between two propagation steps. In the 3-D case, the rules for planar simulations are applied along the boundary normal, in the corners along the 45° direction between the edges of the computational window. However, all potential pitfalls of TBC (see e.g. Ref. [6]) are inherited. The calculations presented below use the more robust STBC field correction described in Ref. [8].

For some structures computational instabilities have been observed if the original corrections [8] were used. These instabilities vanished if the field correction procedure was switched off. They can be reduced or avoided with one or both of the following modifications (cf. Ref. [9]):

- More than two points in the neighbourhood of the boundary are used to determine the factor $\exp(-ik_x\Delta x)$ [8]. Each pair of neighbouring points gives different ratios $\exp(-ik_x\Delta x)$. The field at the boundary is reset by applying the average of these factors.
- The factor $\exp(-ik_x\Delta x)$ is normalized before the field is corrected:

$$\exp(-ik_x\Delta x) \rightarrow \exp(-ik_x\Delta x)/|\exp(-ik_x\Delta x)|.$$

Both modifications result in a slightly reduced transparency in test calculations with Gaussian beams, but they guarantee a stable algorithm.

Note that stability is a property of the entire numerical procedure. It also depends on the structure of interest, the operation wavelength, the mesh stepsizes and the parameter α in Eq. (5).

In the following text we denote by WFBC the Wave

Fitted Boundary conditions as described above. WFBC* indicates that the field correction procedure between two propagation steps has been switched off.

Very recently a somewhat similar method (Uniform Absorbing Boundary Conditions UABC) has been published [16]. It is based on an ansatz like Eq. (7) for the second transverse derivative $\partial_x^2\psi$ only. The unknown coefficients are determined to model a few suitably selected outgoing plane waves exactly. However, the discussion remains restricted to two dimensional problems in homogeneous space.

V. NUMERICAL RESULTS

A few simple examples are presented in order to justify some rather arbitrary assumptions of the previous Section.

A. 2-D Gaussian Beams

Properly adjusted boundary conditions should not have any effect on light beams propagating at small angles towards the boundary. The power on the computational window should vanish after a sufficiently large propagation distance $N_z\Delta z$ and there should be no distortion of the field profile when the beam is leaving the domain. With the initialisation

$$\psi(x, 0) = \exp(-(x - x_s)^2/x_w^2) \exp(-i(kn \sin \beta)x) \quad (13)$$

a Gaussian beam of width $2x_w$ centered at x_s is launched, which propagates at an angle β with respect to the z -direction. In the following the reflection coefficient $R = P^{N_z}/P^0$ with $P^s = \sum_{a=1}^{N_x} |\psi_a^s|^2$ is used to measure the transparency of the boundary.

Parameters for the first test simulation are similar to Ref. [8]: $\lambda = 2\pi/k = 0.828 \mu\text{m}$, $n = n_r = 1.0$, computational window: $[-25.0 \mu\text{m}, 25.0 \mu\text{m}]$ with 256 discretization points, $\Delta x = \Delta z = 0.2 \mu\text{m}$, $N_z = 5000$ corresponding to a distance of $1000 \mu\text{m}$ for beams with $x_w = 10.0 \mu\text{m}$, $x_s = 0$ and $\beta \geq 5^\circ$. Concerning the undetermined parameters in Eq. (9) and (11) the following results have been obtained (note that φ does not appear in the 2-D case):

- θ_{max} enters through the density of the θ_l values. It has only a small influence on the reflection coefficients. We have set $N_\theta = 100$, $\theta_{max} = 30^\circ$.
- θ_w has only a marginal influence on R as well. For a properly chosen θ_{opt} a small angle works best: $\theta_w = 2^\circ$.
- θ_{opt} is the crucial parameter in this list. The value has to be set up in such a way that low reflection coefficients are obtained for paraxial angles β between 0° and 12° , say. This dependence is shown in Fig. 4. For each angle β , the boundary conditions fitted to a θ_{opt} close to β work best, for small angles even better than the TBC. The following planar waveguide simulations use the value $\theta_{opt} = 7.5^\circ$.

However, for a given value of θ_{opt} there are always propagation angles for which the reflection coefficient of the WFBC* is much larger than that of the TBC. The values are lowered to the TBC level if the TBC field correction

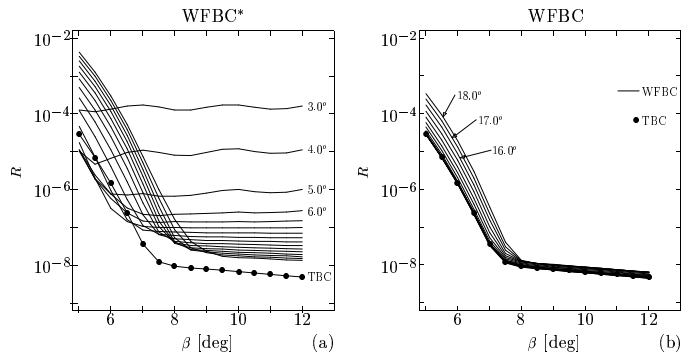


Fig. 4. Reflection coefficients R for WFBC* (a) or WFBC (b) and TBC versus the propagation angle β . Parameter is θ_{opt} . The curves start with $\beta = 5^\circ$ because beams at smaller angles do not pass the boundary within the given propagation distance.

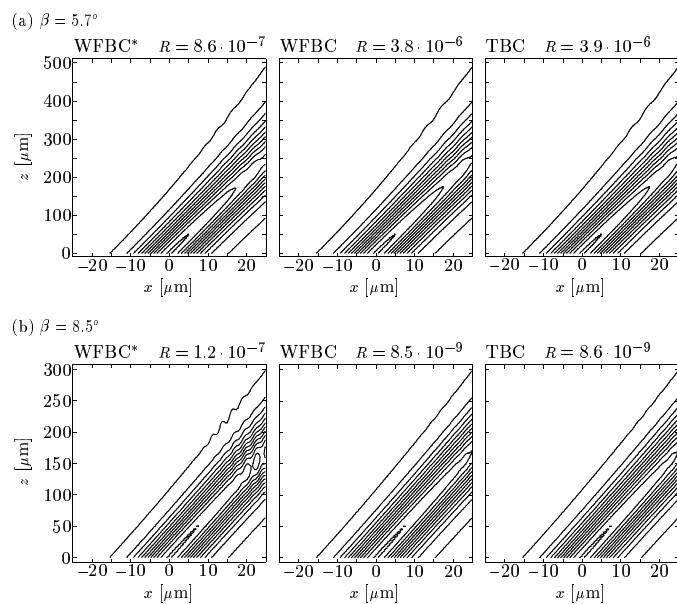


Fig. 5. Contour plots for $|\psi|^2$. Gaussian beams with angles 5.7° (a) and 8.5° (b) are launched at $z = 0$. The reflection coefficients correspond to a distance of $1000 \mu\text{m}$.

[8] is switched on (see Fig. 4). In particular, the strong dependence on θ_{opt} vanishes and the adaptive character of the TBC is transferred to the WFBC. The new boundary conditions may be used for arbitrary fields without special adjustment. Fig. 5 shows some field profiles computed with different boundary types and beam angles.

B. Planar Waveguides

When a Gaussian beam is launched into a guiding structure, a certain amount of power is radiated away and should leave the computational window. This situation may serve to compare the effect of the WFBC and TBC when employed for waveguide simulations. Fig. 6 sketches the structure under consideration. The WFBC use a modification in the field corrections: The factors $\exp(-ik_x \Delta x)$ are averaged over two pairs of field values next to the boundary points.

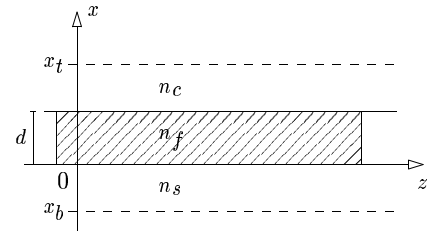


Fig. 6. Planar waveguide used for the simulations in Section 5.B. Parameters are: refractive indices $n_c = 1.0$, $n_f = 2.3$, $n_s = 1.95$, thickness $d = 0.6 \mu\text{m}$, wavelength $\lambda = 1.3 \mu\text{m}$; computational window $x_b = -1.975 \mu\text{m}$, $x_t = 1.975 \mu\text{m}$; mesh $N_x = 80$, $\Delta x = 0.05 \mu\text{m}$, $\Delta z = 0.05 \mu\text{m}$, $\alpha = 0.51$. $n_r = 2.141$ is set to the effective refractive index of the single TM-polarized Mode.

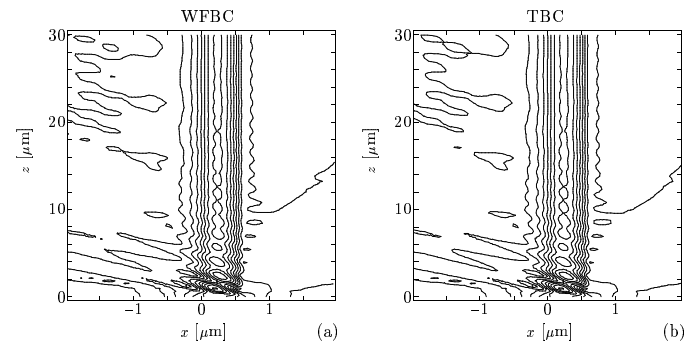


Fig. 7. Contours of $|H_y|$ for the waveguide of Fig. 6, calculated with the WFBC method (a) and the TBC algorithm (b). A Gaussian profile (13) with parameters $x_w = 0.6 \mu\text{m}$, $x_s = 0.3 \mu\text{m}$, $\beta = 0^\circ$ is used as an initial field at $z = 0$.

Fig. 7 illustrates the computed fields if excitation by a Gaussian beam is modeled. Only marginal differences between the contours generated with TBC and WFBC are visible.

If the input field is varied, different amounts of power must cross the boundary of the computational window. Fig. 8 shows the remaining (relative) power, it contains curves for both boundary procedures. The results obtained with TBC and WFBC agree very well, differences remain below $2 \cdot 10^{-3}$. Both algorithms are fast, the new one being four times faster.

If the computational window is enlarged (at constant transverse stepsize), the field and therefore the power on the original window should remain unaltered. For a WFBC computation similar to Fig. 7, but with 240 mesh points instead of 80, the power within the old window deviates by less than $2 \cdot 10^{-3}$ — a remarkable result.

C. 3-D Calculations

The initial field

$$\psi(x, y, 0) = \exp(-x^2 + y^2)/x_w^2) \cdot \exp(-ikn((\sin \beta)x + (\cos \beta \sin \gamma)y)) \quad (14)$$

launches a Gaussian beam with radius x_w at angles β and γ with respect to the z axis. It propagates in free space. According to investigations comparable to Section 5.A the

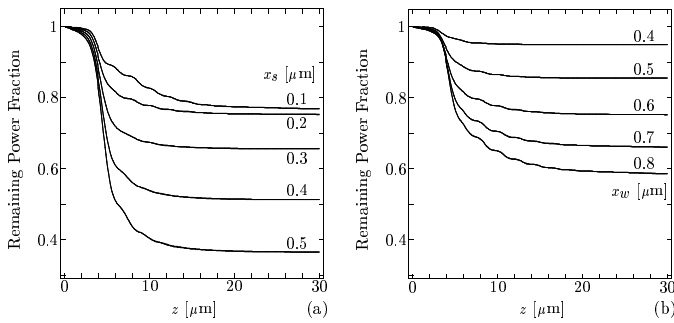


Fig. 8. Power within the computational window versus the propagation distance z for the waveguide of Fig. 6. Gaussian profiles (13) of varying shapes are launched. Parameters are $x_w = 0.6 \mu\text{m}$, $\beta = 0^\circ$ (a) and $x_s = 0.2 \mu\text{m}$, $\beta = 0^\circ$ (b). The curves belong to different values of x_s [μm] (a) and x_w [μm] (b).

new boundary conditions work properly with the following parameters:

$$\theta_{opt} = 10.5^\circ, \theta_w = 5.0^\circ, \theta_{max} = 30.0^\circ, N_\theta = N_\varphi = 80.$$

Fig. 9 exhibits practically no distortion of the Gaussian profile where the beam crosses the boundary of the computational window. A reflexion coefficient of 4.1×10^{-6} is obtained, for a propagation distance of $N_z \Delta z = 400 \mu\text{m}$. The program consumes 14 min CPU-time (HP-715/50 workstation), 4 min are spent with the LU-decomposition of the propagation matrix. If the LU-decomposition were necessary after every step, the program would have to run for more than two days.

The new boundary conditions have been developed in the context of heavy requirements: fully vectorial, magneto-optic (gyrotropic) material, lack of supercomputers. Three complex components of the magnetic field have been propagated in longitudinally homogeneous rib waveguide structures, such as nonreciprocal phase shifters or nonreciprocal couplers [17]. In a typical situation ($60 \times 70 \times 3 = 12600$

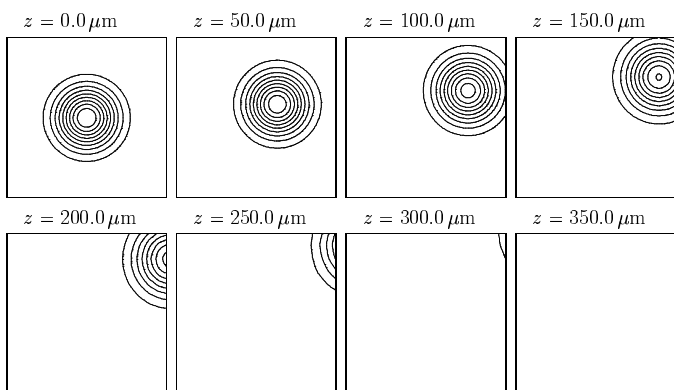


Fig. 9. Propagation of a Gaussian beam (14). Lines with constant $|\psi|$ are shown. The frames of each picture indicate the boundary of the computational window. Parameters are: $x_w = 9 \mu\text{m}$, $\beta = 5^\circ$, $\gamma = 8^\circ$, $\lambda = 0.825 \mu\text{m}$, $n = n_r = 1.0$; computational window $50 \mu\text{m} \times 50 \mu\text{m}$, $N_x = N_y = 100$, $\Delta x = \Delta y = 0.5051 \mu\text{m}$, $\Delta z = 0.5 \mu\text{m}$.

field variables, 63708 propagation matrix entries) the ratio of LU-decomposition to backsubstitution is 400 (CPU-time). Runtimes of hours with our new boundary conditions would have required fortnights with TBC, on the same computer. However, this advantage may become less impressive if other specialized equation solvers and corresponding approximations (e.g. splitting the transverse Laplacian to obtain tridiagonal matrices) can be employed [18], [19].

VI. CONCLUSIONS

We propose a new approach to implementing transparent boundary conditions for finite difference beam propagation simulations. Our method provides difference schemes for boundary points which leave the propagation matrices unchanged within longitudinally homogeneous sections. The boundary conditions do not require tedious adjustments since refractive indices and mesh parameters are involved only. No additional resources of runtime and memory are spent for dealing with the boundary of the computational window. In most cases, runtimes are reduced considerably. Our method comes close to or draws up with the performance of Hadley's transparent boundary conditions without the drawback of having to modify the propagation matrix after every propagation step. In contrast to some other procedures the new method is applicable to fully vectorial three-dimensional simulations without the need to split the transverse Laplacian.

Maybe the basic idea – to adjust the finite difference scheme such that plausible generating functions are reproduced – may be of interest to other efforts to solve partial differential equations by the finite difference method.

ACKNOWLEDGMENTS

Financial support by Deutsche Forschungsgemeinschaft (Sonderforschungsbereich 225 and Graduiertenkolleg 'Mikrostruktur oxidischer Kristalle') is gratefully acknowledged.

REFERENCES

- [1] D. Yevick, "A guide to electric field propagation techniques for guided-wave optics," *Optical and Quantum Electronics*, vol. 26, pp. 185–197, 1994.
- [2] M. D. Feit and J. A. Fleck, "Light Propagation in Graded-Index Optical Fibers," *Applied Optics*, vol. 17, no. 24, pp. 3990–3998, 1978.
- [3] P. E. Lagasse and R. Baets, "The Beam Propagation Method in Integrated Optics," in *Hybrid Formulation of Wave Propagation and Scattering*, L. B. Felsen, Ed., Dordrecht, Boston, Lancaster, 1984, pp. 375–393, Martinus Nijhoff Publishers.
- [4] V.A. Baskakov and A.V. Popov, "Implementation of transparent boundaries for numerical solution of the Schrödinger equation," *Wave Motion*, vol. 14, pp. 123–128, 1991.
- [5] R. Accornero, M. Artiglia, G. Coppa, P. Di Vita, G. Lapenta, M. Potenza, and P. Ravetto, "Finite difference methods for the analysis of integrated optical waveguides," *Electronics Letters*, vol. 26, no. 23, pp. 1959–1960, 1990.
- [6] G. Hugh Song, "Transparent boundary conditions for beam-propagation analysis from the Green's function method," *Journal of the Optical Society of America A*, vol. 10, no. 5, pp. 896–904, 1993.
- [7] G. R. Hadley, "Transparent boundary condition for beam propagation," *Optics Letters*, vol. 16, no. 9, pp. 624–626, 1991.

- [8] G. R. Hadley, "Transparent Boundary Condition for the Beam Propagation Method," *IEEE Journal of Quantum Electronics*, vol. 28, no. 1, pp. 363-370, 1992.
- [9] D. Yevick, J. Yu, and Y. Yayon, "Optimal absorbing boundary conditions," *Journal of the Optical Society of America A*, vol. 12, no. 1, pp. 107-110, 1995.
- [10] W. Huang, C. Xu, S. Chu, and S. K. Chaudhuri, "The Finite Difference Vector Beam Propagation Method: Analysis and Assessment," *Journal of Lightwave Technology*, vol. 10, no. 3, pp. 295-305, 1992.
- [11] Y. Chung and N. Dagli, "An Assessment of Finite Difference Beam Propagation Method," *IEEE Journal of Quantum Electronics*, vol. 26, no. 8, pp. 1335-1339, 1990.
- [12] A. Erdmann and P. Hertel, "Beam-Propagation in Magneto-optic Waveguides," *IEEE Journal of Quantum Electronics*, vol. 31, no. 8, pp. 1510-1516, 1995.
- [13] K. S. Kundert, "Sparse User's Guide: A Sparse Linear Equation Solver," (Version 1.3.a). Department of Electrical Engineering and Computer Sciences, University of California, Berkeley.
- [14] C. Vassallo, "Reformulation for the Beam Propagation Method," *Journal of the Optical Society of America*, vol. 10, no. 10, pp. 2208-2216, 1993.
- [15] D. Yevick and M. Glasner, "Analysis of forward wide-angle light propagation in semi-conductor rib waveguides and integrated-optic structures," *Electronics Letters*, vol. 25, pp. 1611-1613, 1989.
- [16] C. Vassallo and F. Collino, "Highly Efficient Absorbing Boundary Conditions for the Beam Propagation Method," *Journal of Lightwave Technology*, vol. 14, no. 6, pp. 1570-1577, 1996.
- [17] A. Erdmann, M. Shamonin, P. Hertel, and H. Dötsch, "Finite difference analysis of gyrotropic waveguides," *Optics Communications*, vol. 102, no. 1,2, pp. 25-30, 1993.
- [18] A. Kunz, F. Zimulinda, and W. E. Heinlein, "Fast Three-Dimensional Split-Step Algorithm for Vectorial Wave Propagation in Integrated Optics," *IEEE Photonics Technology Letters*, vol. 5, no. 9, pp. 1073-1076, 1993.
- [19] W. P. Huang and C. L. Xu, "Simulation of Three-Dimensional Optical Waveguides by a Full-Vector Beam Propagation Method," *IEEE Journal of Quantum Electronics*, vol. 29, no. 10, pp. 2639-2649, 1993.